

# The Use of Birefringence for Predicting the Stiffness of Injection Molded Polycarbonate Discs

N. M. NEVES and A. S. POUZADA

*Department of Polymer Engineering  
Universidade do Minho  
4800 Guimarães, Portugal*

and

J. H. D. VOERMAN and P. C. POWELL

*Chair of Eng. Design With Plastics, Dept. of Mech. Eng.  
University of Twente  
7500 AE Enschede, The Netherlands*

Polycarbonate discs were injection molded with different sets of molding conditions. The parameters studied were the flow rate, melt- and mold-temperature. The discs were subjected to three point support flexural tests. Those tests are specially intended for injection molded discs because of their inherent non-flatness. The through-thickness molecular orientation was assessed by birefringence measurements along and across the flow direction using the wedge method. This method is ideal to measure the birefringence of materials that are difficult to cut with a microtome. The through-thickness stiffness of the discs was calculated from the measured birefringence distributions. A composite model of the disc was used in the Algor finite element method (FEM) package to simulate the flexural tests.

## 1. INTRODUCTION

Injection molded products exhibit anisotropic morphology induced by the complex thermomechanical history during processing. One of the main features of that morphology is the distribution of molecular orientation. The molecular orientation arises when chain segments showing preferential directions of alignment are unable to relax owing to the fast cooling through the glass transition temperature ( $T_g$ ). The alignment of the chains is a result of the flow-induced stress field that develops during the filling, packing and holding stages of the process. Since the time to cool down to below  $T_g$  increases from the wall towards the center of the part, the pressure- and thermal-induced stresses during cooling build up a distribution of molecular orientation in that direction (1-3).

The flow shear stresses are bigger near the wall than in the core. The shear stresses tend to align the chain segments in the flow direction. In the core, where the flow is divergent, stretching will occur, and the material tends to align in the direction transverse to the flow (4). Since the skin is in contact with the cold mold wall, the molecular orientation in this region freezes almost instantaneously. Some of the molecular orientation will relax, but close to the skin the time for

relaxation is short. These conditions lead to high level of molecular orientation in the skin. In the core, the shear stresses applied to the melt are smaller and the time for molecular orientation relaxation is longer, thus, the level of molecular orientation is lower.

In the case of a disc injected in the center, the state of molecular orientation is a result of the mechanisms described above. At constant flow rate, the linear speed of the flow front decreases towards the end of the flow path, this leading to a complex point to point variation of molecular orientation (5-7).

The molecular orientation induces anisotropy, since some mechanical properties (e.g. stiffness) are increased in the direction of alignment in relation to those in transverse direction (8). The distribution of molecular orientation across the thickness and along the flow path results in a variation of mechanical properties in those directions.

Birefringence is the most widely used property for the assessment of molecular orientation in polymers. With this technique it is possible to obtain quantitative results that can be related to the molecular orientation and the residual stresses (2, 6, 9). The birefringence is measured using polarized light microscopy. The most common method to measure the birefringence makes

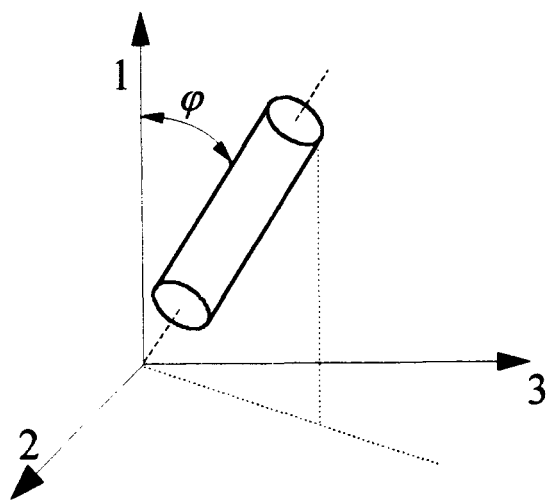


Fig. 1. The orientation of a chain unit with respect to the flow direction (1-axis) represented by the angle  $\varphi$ .

use of a compensator to numerically assess the optical path difference. When sample preparation by microtoming is difficult as it is in polycarbonate, the wedge method is preferred (10). This method makes use of the optical path difference linear relationship to the thickness, to calculate the birefringence. If the wedge specimen is observed with monochromatic polarized light, a set of dark fringes regularly spaced will be visible. The birefringence can be calculated from the distance between consecutive fringes, the angle of the wedge, and the wavelength of light (10-12), using the following expression:

$$\Delta n = \frac{\lambda}{l \tan \theta} \quad (1)$$

where

- $\lambda$  — wavelength of light
- $l$  — distance between two consecutive fringes (Fig. 3b)
- $\theta$  — angle of the wedge

In injection molded products, the birefringence depends on the molecular orientation and on the residual stresses. Three major sources of residual stresses have been identified: thermal- and pressure-induced stresses and frozen-in entropic stresses (4). The frozen-in entropic stresses are related to the non-randomness of the chain orientation. The inhomogeneous cooling and the volumetric changes associated to the variation of properties during cooling result in a distribution of thermal stresses across the thickness direction. Those stresses have a parabolic distribution already observed in quenched specimens, being compressive at the wall and tensile in the center (13, 14). The pressure-induced stresses were associated to a tensile peak in the residual stresses near the wall, which is typical of injection molded products (3, 15, 16). The thermal stresses are generally higher than the entropic stresses, and of the same order of magnitude of the pressure-induced stresses.

The stiffness of the molding in a given direction can be estimated knowing the molecular orientation, in that direction. The molecular orientation can be determined by birefringence measurements (8, 17). However, the birefringence measured in as molded specimens has the contribution resulting from the residual stresses, since

$$\Delta n = \Delta n_{or} + \Delta n_{str} \quad (2)$$

where the subscripts *or* and *str* refer to orientation and residual stresses, respectively. If the magnitude of the residual stresses is known, their contribution to the birefringence can be subtracted using the stress-optical coefficient (6).

If the molecules are symmetrically aligned around the flow direction, 1-axis (Fig. 1), according to a statistical distribution of the angle  $\varphi$  adapted from the kinetic theory of rubber elasticity (18), an orientation averaged relation between the compliance of the material and the state of molecular orientation can be obtained:

$$\frac{S_{//} - S_{//\infty}}{S_0 - S_{//\infty}} \cong \frac{3}{2} \overline{\sin^2 \varphi} \quad (3)$$

where

- $S_{//\infty}$  — Compliance of the material fully aligned
- $S_0$  — Compliance of randomly aligned material

A comprehensive description of the theory that leads to Eq 3 can be followed in reference (8). Introducing the Hermans orientation factor that relates the birefringence to the state of orientation of the segments in relation to the 1-axis (19),

$$f_H = \frac{\Delta n_{or}}{\Delta n_{or\infty}} = 1 - \frac{3}{2} \overline{\sin^2 \varphi} \quad (4)$$

where

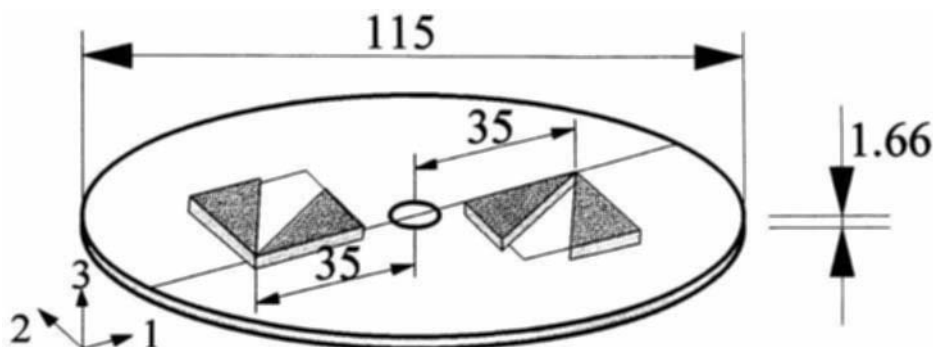
- $\Delta n_{or}$  — Birefringence of the material
- $\Delta n_{or\infty}$  — Birefringence of the material fully oriented

the expression (3) may be simplified assuming that  $S_{//\infty}$  is negligible because it is much smaller than  $S_{//}$  and  $S_0$ . Thus, combining (3) with (4) and transforming compliance into stiffness, it results

$$E_{//} = E_0 \left( 1 - \frac{\Delta n_{or}}{\Delta n_{or\infty}} \right)^{-1} \quad (5)$$

which is in good agreement with experimental results (8). This expression will enable the prediction of stiffness from experimental birefringence data. About the assumption ( $S_{//\infty} \approx 0$ ) made to obtain Eq 5, in fact it is not easy to obtain a value for  $S_{//\infty}$ , however we can discuss the order of magnitude of the error introduced. If we accept that the modulus of the fully oriented material is at least five times the modulus of unoriented material, and the birefringence is lower than  $10^{-3}$  (smaller values were found in literature), then the maximum error in using the Eq 5 will be of 2.5%.

Fig. 2. Specimens cut from each disc.



## 2. EXPERIMENTAL

Centrally gated discs (Fig. 2) were molded in a 600 kN Krauss Maffei 60/210A injection molding machine. The mold was used before for reproducing morphological features of typical commercial moldings of semi-crystalline materials. The gate diameter is 7.5 mm, which can be considered large for this size of molding, and it is likely to lead to a higher orientation gradient in transverse direction and a lower overall level of orientation and stiffness. The material used was a general purpose polycarbonate grade from GEP, Lexan 141 R. The molding program and the codes used are summarized in Table 1.

### 2.1 Birefringence Measurements

Two discs per molding condition were used for birefringence determination. In each disc four triangular specimens were cut at 35 mm from the center, two along and two across the flow direction (Fig. 2). These testpieces should have approximately 30°/60°/90° angles.

The testpieces were polished in the two longer edges, to remove any cutting marks left. Then they were mounted into a bath of paraffin to reduce the

reflection from the surface and improve the image contrast, as shown in Fig. 3a.

Green light of 550 nm wavelength was used. The birefringence was determined from data obtained from acquired fringe patterns with a Leica Quantimet 500 image analyzer. Over twenty points across half thickness were measured. Symmetry across the thickness was verified in some specimens and just visually assessed in the remaining. Data was obtained from the average of four specimens.

### 2.2 Flexural Tests and Simulation

The flexural stiffness of the discs in the three-point support flexural test (designed for overcoming the inherent non-flatness of molded plates) is assessed in three ways: a) experimentally, b) using an analytical solution for an isotropic material, with data from the raw material manufacturer, and c) using a FEM package with a laminate model, with data calculated from birefringence. The flexural tests were carried out with an Instron tensile test machine equipped with a specific jig as described elsewhere (20). The tests were made at 1 mm/min crosshead speed to the maximum displacement of 0.8 mm (about half thickness of the specimens) to keep the test in the proportional elastic strain region. The environment was kept at 23°C with the relative humidity at 55%. Seven specimens were tested per molding condition.

### 2.3 Isotropic Solution

The Bassali equation (21) solves analytically the problem of a flexed isotropic disc simply supported in a finite number of support points placed in the outer rim of the disc. For the case of three points of support defining a radius smaller than the radius of the disc, a stiffness correction is needed. That correction was defined elsewhere (22).

In the isotropic solution it was assumed that the isotropic elastic constants were independent from the processing conditions which only affected the overall thickness of the moldings (Table 1).

### 2.4 FEM Simulation

A 936 quadrilateral composite elements model was created using the Algor software (23) to simulate the

Table 1. Molding Program and Codes.

Code	Melt Temperature (°C)	Injection Flow Rate cm <sup>3</sup> /s	Mold Temperature (°C)	Thickness (mm)
A	280	10	80	1.622
B		20		1.631
C		40		1.687
D	300	10	80	1.695
E		20		1.649
F		40		1.670
G	310	10	100	1.691
H		20		1.738
I		40		1.779
J	280	20	80	1.660
K	280		100	1.653
L	300		100	1.649
M	310	120	120	1.668
N	310			1.661

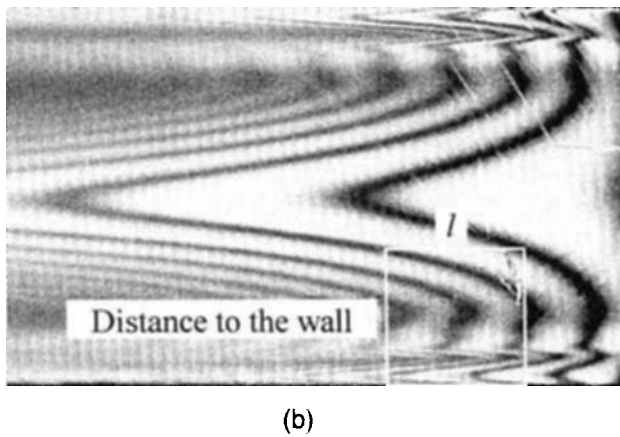
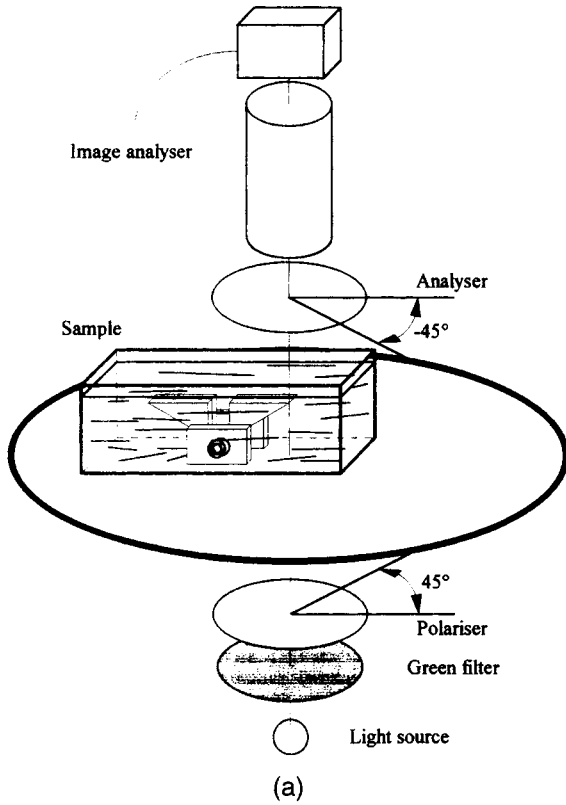


Fig. 3. Birefringence experiments: a) apparatus; b) measurement from fringe patterns.

flexural tests (Fig. 4). The boundary conditions were defined in the support points (shown as circles in Fig. 4), constraining the out of plane translation of those nodes. The load is applied at the center of the disc.

For applying the FEM code, the moldings were considered to be made of 12 layers symmetrically distributed with respect to the midplane surface (Fig. 5). For the simulations each layer was considered to be orthotropic with respect to radial and tangential directions. The definition of the layers was intended to describe the variation of properties with the smallest number of layers. In Fig. 5 it is exemplified the case of molding A, where the non-constancy of the layer thick-

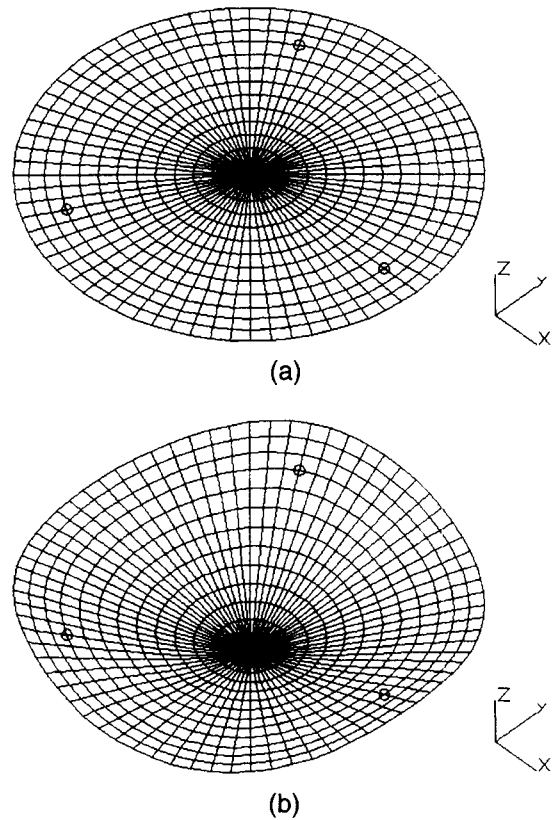


Fig. 4. Algor model for simulation of flexural tests a) undeformed mesh, b) deformed plate, scale set to 25. Circles are supports; load applied in center point.

ness is evident. The stiffness is calculated from birefringence through Eq 4, using  $\Delta n_{or_{\infty}} = 0.062$ , from (8) and a stiffness  $E_0 = 2.3$  GPa, from manufacturer's data.

The flexural behavior of transversely loaded plates is not very sensitive to small variations of the lateral contraction ratio. It was assumed that the major lateral contraction ratio,  $\nu_{12}$ , is of the order of the manufacturer's quoted average Poisson's ratio, 0.38.

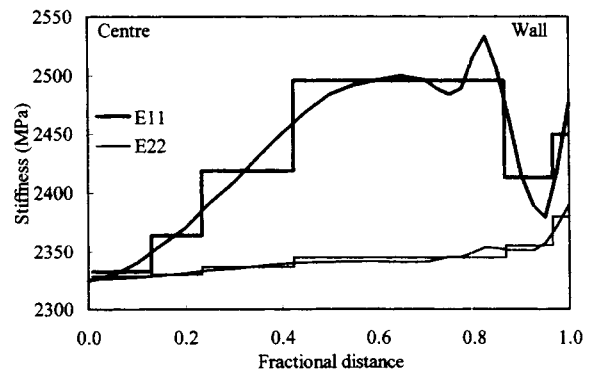


Fig. 5. Layers stiffness discretized from through-thickness birefringence distributions, sample A.  $E_{11}$  is the along flow stiffness and  $E_{22}$  is the across flow stiffness.

Table 2. Slope of Force/Deflection in Flexural Tests and Simulations.

	Experimental (Standard Deviation) (kN/m)	Composite FEM Model (kN/m)	Isotropic Solution (kN/m)	Composite FEM Error (%)	Isotropic Error (%)
A	6.64 (0.17)	7.92	8.44	19.3	27.1
B	6.85 (0.16)	8.07	8.58	17.8	25.3
C	9.34 (0.19)	8.91	9.50	-4.6	1.7
D	8.57 (0.19)	9.10	9.63	6.2	12.4
E	8.27 (0.12)	8.91	8.87	7.7	7.3
F	9.10 (0.21)	8.75	9.21	-3.8	1.2
G	9.01 (0.23)	9.00	9.56	-0.1	6.1
H	10.33 (0.15)	9.74	10.38	-5.7	0.5
I	11.73 (0.25)	10.45	11.14	-10.9	-5.0
J	7.76 (0.10)	8.78	9.05	13.1	16.6
K	7.80 (0.11)	8.68	8.93	11.3	14.5
L	8.00 (0.10)	8.57	8.87	7.1	10.9
M	8.65 (0.14)	8.82	9.18	2.0	6.1
N	8.46 (0.23)	8.73	9.06	3.2	7.1

The comparison between the experimental results and the simulation is based in the slope of the force-displacement curve. Results obtained with the analytical solution for isotropic materials are reported in Table 2 as well.

### 3. BIREFRINGENCE RESULTS AND DISCUSSION

The results of birefringence are depicted in Figs. 6 to 8. The experimental uncertainty is bigger near the wall, since the minor angle of the wedges ( $\sim 30^\circ$ ) is not constant because of mechanical damage during the polishing stage. Maximum variation of  $5^\circ$  was obtained on measuring that angle. This angular variation can result in errors up to 18% upon calculating birefringence.

#### 3.1 Gapwise Radial Birefringence

Three local maxima can be observed in the gapwise birefringence,  $\Delta n_{13}$ , independently from the molding temperature, Figs. 6a-6c. The first, which will be referred to as wall maximum, appears near the wall and has been associated with the fountain flow that develops during the filling stage (1). However, recent developments (4, 15, 16) show that this wall maximum depends on the pressure applied during the packing and holding phases of the injection cycle. In fact, here, where these pressures were not changed, little variation on the magnitude of this peak was observed. The second maximum develops in the filling shear region. The magnitude of the shear peak depends on the flow rate as well as its distance from the wall. The third maximum has been ascribed to the flow during the packing and holding stages, and to the pressure applied to the melt during those stages; it will be referred to as the packing peak. The molding parameters seem to have no effect on the birefringence at the center. The birefringence at the center has been associated with the residual stresses present in the specimen. Recently that birefringence was attributed to transient stresses that became frozen in during vitrification (4).

The flow rate has major effect in the gapwise radial birefringence. Lower flow rates result in higher shear peak and packing maxima, the effect being more noticeable at low melt temperatures. Flow rate seems to be the most important molding parameter to determine the gapwise birefringence, which varies inversely to it.

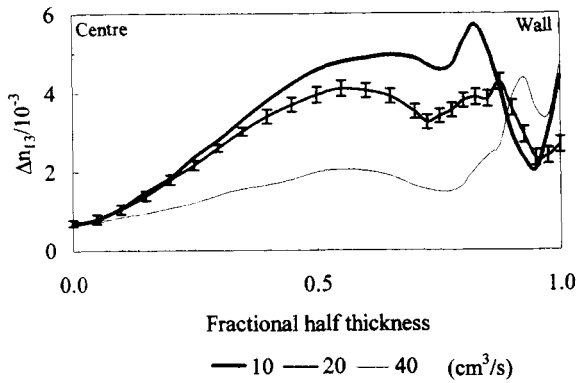
Higher melt temperature lead to lower values of radial birefringence, as can be observed in Fig. 7. The melt temperature has limited effect on the through thickness position of the three birefringence maxima.

#### 3.2 Gapwise Tangential Birefringence

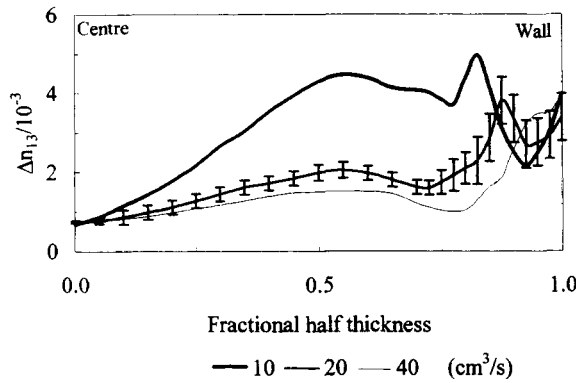
At the wall and in the center the studied parameters have no significant effect on the tangential birefringence  $\Delta n_{23}$ , Fig. 8. The same behavior was observed in compact discs of polycarbonate (4).

In Fig. 8a it can be observed that the flow rate affects the birefringence of the intermediate region. The same qualitative behavior is evident in Fig. 8b and 8c, but as the melt temperature increases the quantitative differences are smaller. At  $310^\circ\text{C}$ , the effect of the flow rate is minimum and confined to the region close of the wall. This can be an indication that the thickness of the frozen layer is one of the determining parameters in the building up of transverse birefringence. The tangential birefringence appears to be rather insensitive to the melt temperature as shown in Fig. 9.

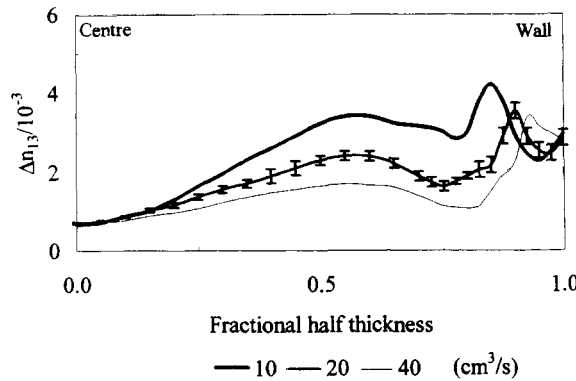
Those results of birefringence measurements are in qualitative agreement with similar experiments reported by Wimberger-Friedl (6) using compact discs of polycarbonate. In quantitative terms the birefringence distributions in flow direction reported here are consistently higher. This can be explained since the material used in this work is a general purpose grade, whereas the material used for compact discs is a special grade with a lower molecular weight. Thus, lower birefringence levels are to be expected (24). However, the birefringence across flow direction is quantitative and qualitatively very similar. Wu and White (3) reported values for edge gated plates also similar to the



(a)



(b)



(c)

Fig. 6. Variation of gapwise birefringence in flow direction with flow rate at melt temperatures of a) 280°C; b) 300°C and c) 310°C.

ones obtained here using a comparable general-purpose polycarbonate grade, however, with slightly lower viscosity.

### 3.3 The Effect of Mold Wall Temperature on the Birefringence

The mold wall temperature does not affect significantly the birefringence (Fig. 10). An increase of 20°C in the mold temperature, as seen in Fig. 10a, results in a small variation near the wall. Comparing the last

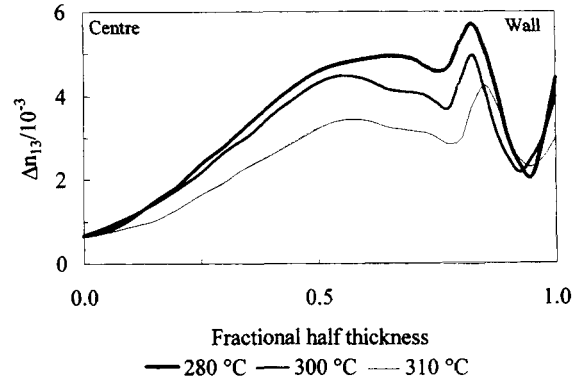


Fig. 7. Variation of gapwise birefringence in flow direction with melt temperature. Flow rate: 10 cm<sup>3</sup>/s.

two curves of 10a, a shift can be observed towards the wall. The mold temperature has limited effect on the tangential birefringence, Fig. 10b.

## 4. FLEXURAL RESULTS AND DISCUSSION

The following aims at evaluating if the flexural behavior of a molded plate can be estimated from morphological features such as birefringence. Of course, birefringence contains a part that is due to residual stresses; however, this will be neglected here. In fact, if we suppose a stress distribution with a tensile maximum of 5 MPa, assuming a stress-optical coefficient of 100 pPa<sup>-1</sup> (8), the maximum birefringence reduction would be of 0.5 × 10<sup>-3</sup>. A compression stress would increase the birefringence. This means that to accurately estimate the stiffness properties from birefringence data it is necessary to study the residual stress, or alternatively, remove the residual stresses. One technique that would enable to separate the two contributions to the birefringence is annealing. However, it has been shown that the relaxation, taking place on annealing below T<sub>g</sub>, does not correlate directly with the residual stresses (6). The reason pointed out for this behavior was the time dependence of the stress optical coefficient. In this work, two specimens (condition J) were subjected to annealing at 130°C during two hours, followed by slow cooling (1°C/min) to room temperature. It was observed a decrease in the birefringence level in the skin and a small decrease of the birefringence in the core. It was observed that the birefringence change was not balanced.

The numerical results for every processing condition used in this work are included in Table 2, where deviations from analytical and FEM predictions are indicated with reference to the experimental data.

The analysis of the results shows that the isotropic solution consistently overpredicts stiffness of the discs for the majority of the molding conditions. Only in the condition I the experimental results show a higher stiffness than predicted. This condition corresponds to an extreme set of parameters (310°C melt temperature and flow rate of 40 cm<sup>3</sup>/s) that tend to create a state of lower molecular orientation and therefore lower bire-

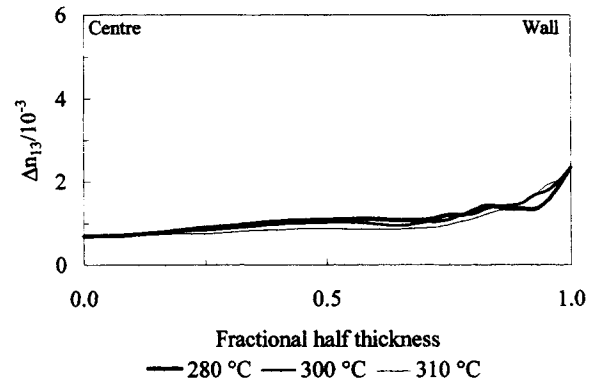
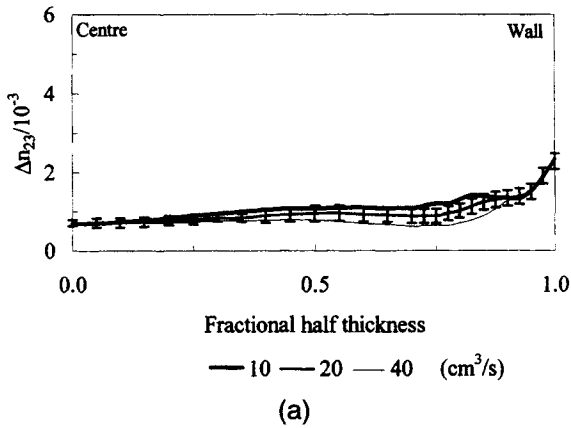


Fig. 9. Variation of gapwise birefringence across flow direction with melt temperature. Flow rate: 10 cm<sup>3</sup>/s.

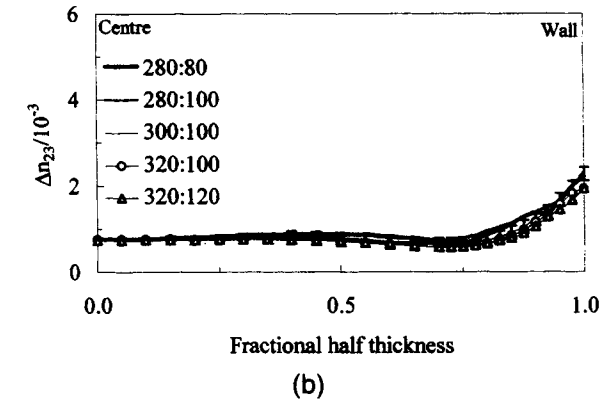
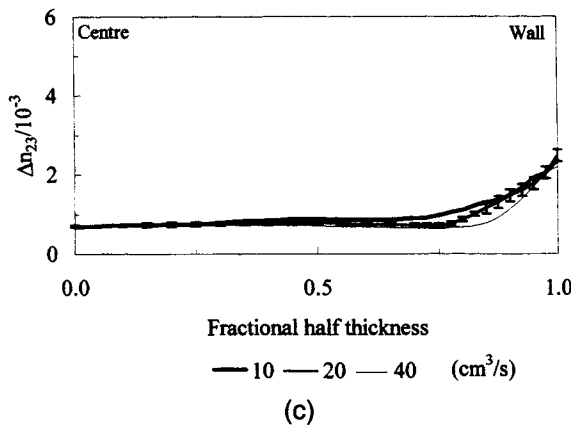
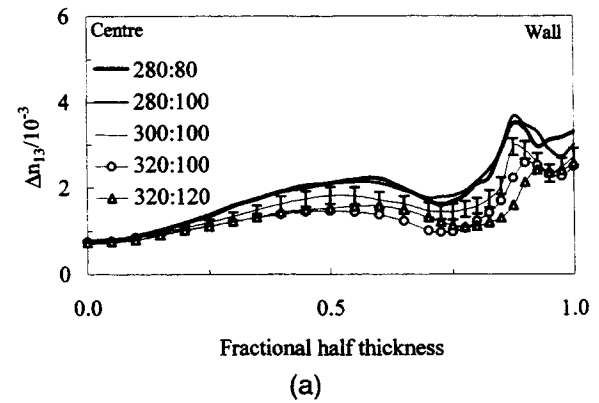
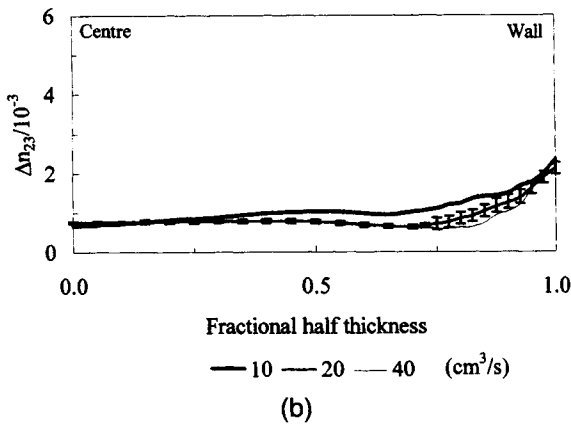


Fig. 8. Variation of gapwise birefringence across flow direction with flow rate at melt temperatures of a) 280°C; b) 300°C and c) 310°C.

Fig. 10. Variation of gapwise birefringence at flow rate of 20 cm<sup>3</sup>/s. Melt temperature: Mold temperature are the parameters, which correspond to molding conditions **J**, **K**, **L**, **M**, and **N**. a) flow direction or 1-3 plane; b) across flow direction or 2-3 plane.

fringence. The molding conditions that lead to smaller deviations between the isotropic model and the experimental results are **C**, **F** and **H**. All these conditions imply flow parameters that favor the isotropy of properties. The birefringence results for these conditions indicate a quasi-equi-biaxial state of orientation.

The FEM simulator also overpredicts the flexural stiffness. However, the approximation of those predictions to the experimental behavior is consistently better than the isotropic model (the molding conditions **C**, **F**, **H**, and **I** are exceptions to the general trend).

The bigger deviations between the experimental results and the FEM simulations are observed for **A**, **B**, **I**, **J**, and **K**. All these moldings, with exception of **I**, were produced with low melt temperature.

Usually closer approximations would be expected from a FEM simulator. It is evident that the consideration of a layered model generally improves the precision. However it must not be forgotten that the layer properties were considered to be constant over the

whole flow path. Also, the effect of the residual stresses was not considered at this stage of the work. The improvement of the method would imply therefore additional experimental work or, more desirably, a model that would predict birefringence from the flow and thermal stress fields.

## 5. CONCLUSIONS

The wedge method is a valuable technique to characterize the birefringence distribution in injection molded products made of rigid materials that may be difficult to prepare by microtoming.

The birefringence distribution through the molding thickness show the three peaks characteristic of polycarbonate moldings. Their magnitude and position depend on molding parameters, namely flow rate and processing temperatures (melt and mold). The increasing flow rate and temperatures cause the birefringence to decrease. In the case of polycarbonate the influence of the mold temperature in birefringence is less noticeable than that of the melt temperature.

The information from birefringence measurements can be used to predict the mechanical behavior of injection molded discs using the Hermans orientation factor to relate birefringence to mechanical characteristics.

The utilization of moduli derived from birefringence measurements to predict the stiffness of injection molded discs using a laminate FEM model led to results within 8% of average error with respect to experimental data. These results are better than using an isotropic model based on manufacturer raw material data. The prediction may be further improved if the birefringence variation along the flow path is introduced and the effect of the residual stresses is deducted in the birefringence data used for calculations.

These findings suggest that birefringence data may be used as a morphological feature to predict the mechanical performance of plates injection molded in amorphous thermoplastics, from the processing conditions.

## 6. ACKNOWLEDGMENTS

N. M. Neves is supported by the Junta Nacional de Investigação Científica e Tecnológica, through a Portuguese-based E. U. program PRAXIS XXI grant, BD 3806/94. The authors gratefully acknowledge Dr. M. J. Oliveira at Universidade do Minho and Dr. D. J. van Dijk and Dr. K. M. B. Jansen at University of Twente for the valuable suggestions and discussions.

## LIST OF SYMBOLS

- $\varphi$  — Angle of a chain unit with respect to the 1-axis (Fig. 1).  
 $\lambda$  — Wavelength of light.  
 $\theta$  — Angle of the wedge in the region of measurement.

- $\Delta n$  — Birefringence.  
 $\Delta n_{or}$  — Birefringence resulting from molecular orientation.  
 $\Delta n_{or\infty}$  — Birefringence of the material fully oriented.  
 $\Delta n_{str}$  — Birefringence resulting from stresses.  
 $f_H$  — Hermans orientation factor.  
 $l$  — Distance between two consecutive fringes (Fig. 3b).  
 $E_0$  — Modulus of randomly aligned material.  
 $E_{11}$  — Modulus along the flow direction.  
 $E_{22}$  — Modulus across the flow direction.  
 $E_{//}$  — Modulus of the material along an arbitrary direction.  
 $S_0$  — Compliance of randomly aligned material.  
 $S_{//}$  — Compliance of the material along an arbitrary direction.  
 $S_{//\infty}$  — Compliance of the material fully aligned.  
 $T_g$  — Glass transition temperature.

## REFERENCES

- Z. Tadmor, *J. Appl. Polym. Sci.*, **18**, 1753 (1974).
- A. I. Isayev, *Polym. Eng. Sci.*, **23**, 271 (1983).
- J.-P. Wu and J. L. White, *Polym. Eng. Sci.*, **31**, 652 (1991).
- R. Wimberger-Friedl, *Int. Polym. Proc.*, **XI**, 4, 373 (1996).
- K. Yoon and K. K. Wang, *SPE ANTEC Tech. Papers*, **37**, 2911 (1991).
- R. Wimberger-Friedl, *Polym. Eng. Sci.*, **30**, 813 (1990).
- G. D. Shyu and A. I. Isayev, *SPE ANTEC Tech. Papers*, **41**, 2911 (1995).
- L. C. E. Struik, *Internal Stresses, Dimensional Instabilities and Molecular Orientations in Plastics*, John Wiley, Chichester, United Kingdom (1990).
- K. M. B. Jansen, *Polym. Eng. Sci.*, **34**, 898 (1994).
- D. A. Hemsley and A. M. Robinson, *Polym. Testing*, **11**, 373 (1992).
- A. H. Wagner, J. S. Yu, and D. M. Kalyon, *Polym. Eng. Sci.*, **29**, 1298 (1989).
- B. P. Saville, *Polarised Light: Theory and Measurements, in Applied Polymer Light Microscopy*, D. A. Hemsley, ed., Elsevier Applied Science, Barking (1989).
- A. Siegman, S. Kenig, and A. Buchman, *Polym. Eng. Sci.*, **27**, 1069 (1987).
- J. R. Saffel and A. H. Windle, *J. Appl. Polym. Sci.*, **25**, 1117 (1980).
- W. F. Zoetelief, L. F. A. Douven, and A. J. Ingen Housz, *Polym. Eng. Sci.*, **36**, 1886 (1996).
- K. M. B. Jansen, *Int. Polym. Process.*, **IX**, 1, 82 (1994).
- I. M. Ward, *Mechanical Properties of Solid Polymers*, 2nd Ed., Wiley-Interscience, Chichester, United Kingdom (1983).
- L. R. G. Treloar, *The Physics of Rubber Elasticity*, 2nd Ed., Oxford University Press, Oxford, England (1967).
- P. H. Hermans, *Physics of Cellulose Fibres*, Elsevier, Amsterdam (1946).
- A. S. D. Pouzada and M. J. Stevens, *Plast. Rubb. Proc. App.*, **4**, 181 (1984).
- W. A. Bassali, *Proc. Camb. Phil. Soc.*, 728 (1975).
- A. S. Pouzada, PhD thesis, Loughborough University of Technology, U. K. (1982).
- Algor Inc., Pittsburgh.
- T. Kanai, K. Shimizu, Y. Uryu, *Int. Polym. Process.*, **IV**, 3, 132 (1989).

Received July 8, 1997  
 Revised October 1997